Pergamon

Cement and Concrete Research 31 (2001) 1191–1202

CEMENT AND CONCRETE RESEARCH

Microscopic analysis of 50% axially strained cementitious materials

Ha-Won Song[a,*], Jang-Ho Jay Kim[b], Jae-Hyeok Choi[a], Keun-Joo Byun[a]

[a]*Department of Civil Engineering, Yonsei University, Shinchon-Dong, 134, Seoul 120-749, South Korea*
[b]*Department of Civil and Environmental Engineering, Sejong University, Seoul 460-0364, South Korea*

Received 18 August 2000; accepted 10 May 2001

Abstract

The microscopic behavior of 50% axially strained cementitious materials is studied. The microscopic behavior of concrete under the triaxial stress condition must be fully understood to explain the additional concrete ductility that comes from lateral confinement and a microstructural mechanism which has been subjected to extreme strain. The so-called "tube-squash" test was used to achieve 50% axial strain and over 70° of shear angle change in a concrete under extremely high pressure, without visible cracks. Then, microscopic analysis focusing on hydration and the microstructure of a 50% axially strained cement paste were performed on cored-out deformed and virgin (undeformed) cement paste specimens; the first specimen was 40 days old and the second one was 1 year old. Field emission scanning electronic microscope (FESEM) analysis was performed to compare the microstructures of the 40-day-old and 1-year-old specimens applied with finite strain. On the 1-year-old specimens, X-ray diffractometer (XRD), energy dispersive X-ray spectrometer (EDS), and differential thermal analysis/thermo-gravity (DTA/TG) analyses were also performed to study the change of hydration and microstructures due to 50% axial strain. The results and implications from these various analyses are discussed.

Keywords: Confined cementitious materials; Tube-squash test; Microscopic behavior; Hydration; Microstructure

1. Introduction

It is a well-known fact that lateral confinement on quasi-brittle materials increases ductility. The additional ductility comes from the enforcement of a triaxial stress state on the quasi-brittle material. In other words, the triaxial stress condition restrains the initiation of tensile cracks and damage localization at stresses far exceeding the tensile strength of the material. In concrete, which is the most widely used quasi-brittle material, the application of confinement by lateral stirrups and the retrofitting of composite wraps are examples of the maximization of ductility. Even under extreme loading conditions such as earthquakes and missile penetration, various types of lateral reinforcement are used to prevent ultimate catastrophic failure and to maintain structural serviceability in concrete structures.

As early as 1905, Woolson [1] discovered that applying lateral reinforcements increases concrete ductility. The results of standard triaxial tests done by Balmer [2] and Bazant et al. [3] also show an increase in concrete ductility due to the lateral confinement. Burdette and Hilsdorf [4] also performed compression tests on concrete columns reinforced by stirrups to show the ductility increase. Park and Paulay [5] proposed constitutive equations considering the confinement effect of concrete, while Bazant et al. [6] experimentally obtained the hydrostatic stress–strain relations of concrete and hardened cement paste up to record pressures of 2069 MPa in confined uniaxial-strain compression tests.

Although the application of confinement to achieve high ductility in cementitious materials has been extensively studied, understanding of the material behavior that causes increased ductility has been lacking. In order to further explain the additional ductility that comes from lateral confinement, the microscopic behavior of cementitious materials under the triaxial stress condition must be fully understood. For example, the way in which the hydration process unfolds during the application of finite strain on hardened cement paste is critical in understanding ductility increase in concrete. After cement paste has been cured, the rehydration between unhydrated or partially hydrated

* Corresponding author. Tel.: +82-2-2123-2806; fax: +82-2-364-5300.
E-mail address: song@yonsei.ac.kr (H.-W. Song).

0008-8846/01/$ – see front matter
PII: S0008-8846(01)00542-7

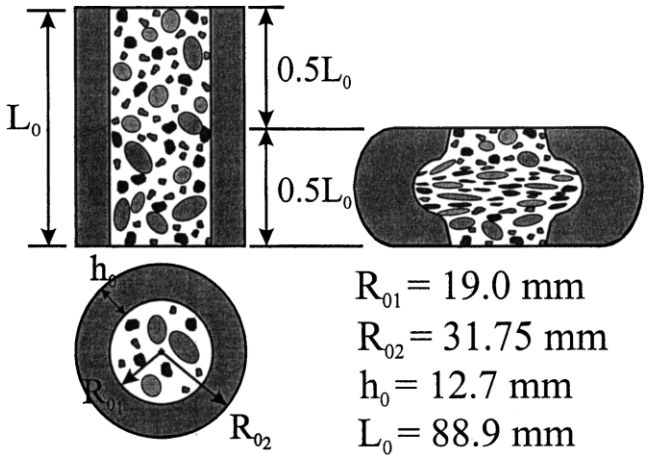

Fig. 1. Schematic tube squash test with 50% axial strain and steel tube dimensions.

cement particles and residual or free water within the hardened cement paste applied with extreme strain has to be further studied. In this study, a microscopic analysis is performed on the 50% axially strained specimens obtained from the so-called "tube-squash test" by Bazant et al. [7]. In his experiment, the cement paste was cast in a highly ductile steel tube and deformed to half of its original length. Then, the inner core of this filled tube specimen was cored out immediately after straining. By applying extreme deformation of 50% axial strain causing over 70° of diagonal shear angle rotation during the straining stage of the experiment, the extreme strained condition was applied to the filled.

In field emission scanning electron microscope (FESEM) analysis, microscopic photos taken from both planar and cross-section specimens of deformed and virgin types obtained after 40 days and 1 year from the initial casting are analyzed. The constituents (C-S-H hydrates, micropores, microcracks, et cetera) of the 1-year-old cement paste specimens are studied using microscopic photos taken at various magnifications, chosen based on the study by Metha and Monteiro [8]. To understand the microstructural behavior of the 50% axially strained cement paste, over 200 photos were taken for the four types of specimens: planar and cross-sectional deformed as well as planar and cross-sectional virgin specimens. X-ray diffractometer (XRD) analysis was also performed on the 1-year-old specimens to compare the relative intensity of $Ca(OH)_2$ in the planar virgin and deformed specimens. In addition, energy dispersive X-ray spectrometer (EDS) analysis was performed on the 1-year-old specimens to understand the changes in molecular distributions and Ca/Si ratio. Finally, differential thermal analysis/thermo-gravity (DTA/TG) analysis was also performed to obtain the quantity of $Ca(OH)_2$ and C-S-H (calcium silicate hydrate) in the microstructures of the 1-year-old specimens. By observing both hydration percentage and microstructure change, the effect of the microstructure change in the 50% axially strained cement paste on increased ductility can be clarified.

2. Experimental work

2.1. Basic characteristics of tube-squash test

All of the tube-squash test results and the specimens used for microscopic analyses are from Bazant's report (Bazant et al. [7]). A series of tests was performed using steel alloy tubes whose dimensions are shown in Fig. 1; the tubes were made of ASTM No. 1020 steel alloy. The mix proportions of high-strength concrete (HSC) and cement paste are shown in Table 1. The HSC had a maximum aggregate size of 9.5 mm, and uniaxial compression strength f_c' of 86.2 MPa. The specimens were cast and cured at room temperature in a water bath for 28 days, after which, they were tested. The tests were carried out at constant rate of axial displacement, which was 2.54×10^{-2} mm/s. A rate higher than 2.54×10^{-2} mm/s was found to be impossible because it caused the steel tube to crack. The specimen diameter was 63.5 mm. The cores drilled out of the specimens were 25.3 mm. Mineralogically, the larger aggregates were clean P-gravels composed mostly of dolomite, granite, basalt, and minimal quartz and metamorphic rock called schist. The sand used in the experiment is normal Number 2 sand. Fig. 2 shows a photo of the compression test setup of the filled tube specimens before and after straining. The specimens were tested using axial displacement control at a constant rate and the axial strain applied to the filled tubes in the tube-squash test is schematically shown in Fig. 1 [7]. When tubes are compressed, as shown in Fig. 3(a), it is important to see the difference between the internal shapes of the filled and empty tubes (Fig. 3(b)). Fig. 3(b) shows a specimen of HSC squashed to 50% of its original length that has been axially cut in the middle. The rearrangement and flattening of the aggregates caused by shortening the filled tube specimen to half of its original length are also shown in the figure. No visual cracks or voids are detected even though initially orthogonal diagonals have changed over 70°. The difference in the internal tube shapes is a result of the extreme internal pressure or hoop stress that the confining steel tube applies to the hardened concrete. Fig. 4(a) shows axial load versus axial and lateral displacements from

Table 1
Mix proportion of HSC and cement paste

Content	HSC	Cement paste
Cement type (kg/m^3)	459.03	1570.52
Agg.-max. 0.625 cm (kg/m^3)	1020.66	
Sand — No. 2 (kg/m^3)	793.66	
S.F. slurry (kg/m^3)	128.11	
Water (kg/m^3)	117.70	628.52
Superplasticizer (ml/m^3)	160.0	

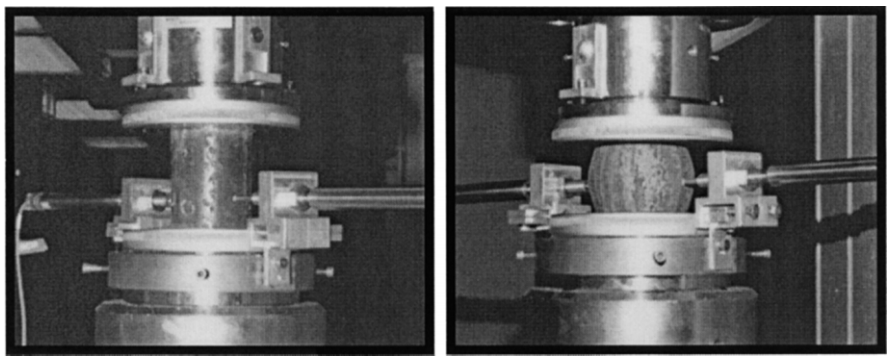

Fig. 2. Photograph before and after compression of filled tube specimen.

the tube squash tests. The plots of the unfilled steel tube compression test results are also shown in Fig. 4(a). The corresponding diagrams of axial stress versus axial and lateral strains for the filled tubes specimens are shown in Fig. 4(b). The results have been discussed in detail in a previous report [7].

Cores with a diameter of 25.3 mm were drilled out of the squashed filled tubes. For the purposes of comparison,

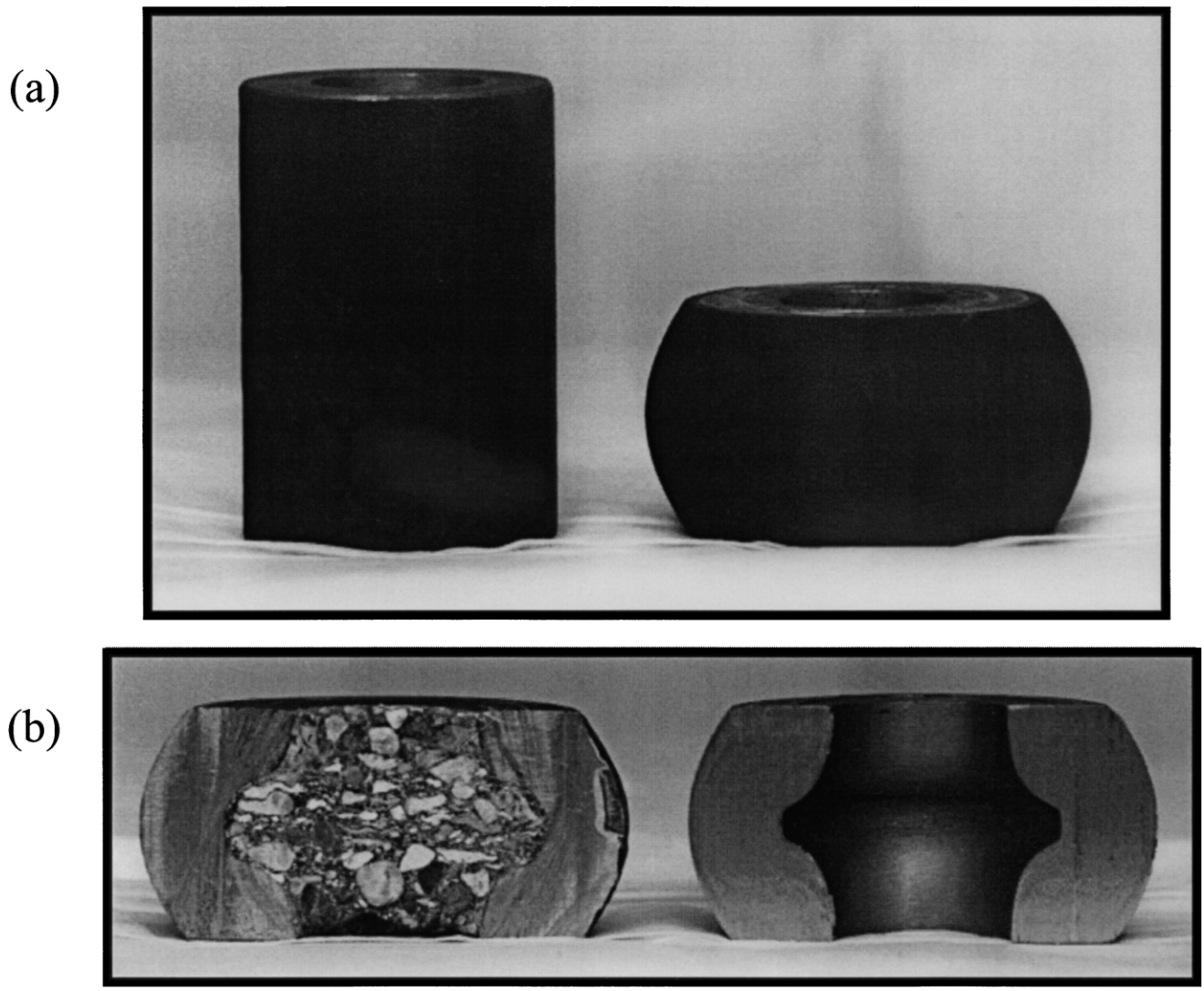

Fig. 3. (a) Comparison before and after compression of steel tube. (b) Comparison of compressed filled tube specimen to compressed hollow steel tube specimen.

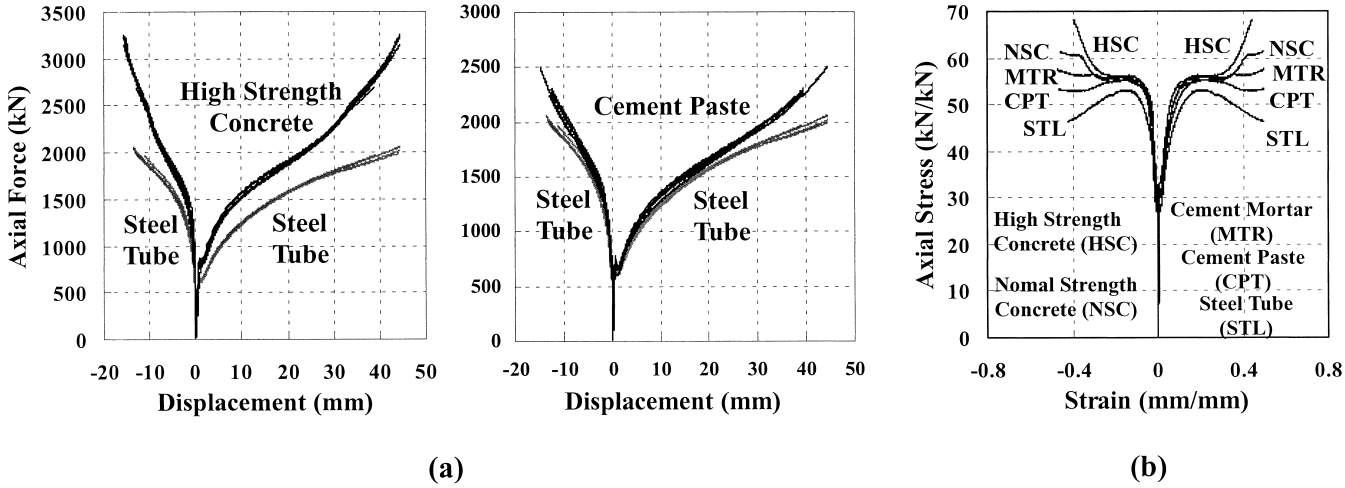

Fig. 4. (a) Axial force versus axial and radial displacement. (b) Axial stress versus axial and radial strain.

identical cores were drilled out of virgin concrete specimens cast from the same batch of concrete used to cast the filled tube specimens. Fig. 5 shows the deformed and virgin core pairs extracted from HSC and hardened cement paste from the filled tubes [7]. In Fig. 5, the deformed and virgin specimens are on the left and right sides of each pair, respectively. After removing the squashed tube specimens from the testing machine, three types of examination are conducted: (1) visual observation, (2) mechanical property testing of core specimens, and (3) microscopic analysis. For visual observation, some filled tube specimens are cut longitudinally and their concrete surfaces are examined visually (Fig. 3(b)). Although the possibility of increasing ductility in concrete by high confining pressure is well known, the strain magnitude that can be attained from the experiment without any visually observable damage is at first startling. Even after undergoing a shear angle change of over 70°, the visual inspection of the surface of the core specimens shows no voids or fractures. These cylindrical cores are then subjected to either uniaxial compression or Brazilian split cylinder tests. A paper by Bazant et al. [7] includes detailed discussions of the results. Among the various types of materials cored out from the tube-squash compression tests, the cement paste cores are used for microscopic analysis.

2.2. Basic characteristics of microscopic analysis

This study is an extension of the study by Bazant et al. [7], mainly focusing on the microscopic analysis of cored-out cement paste specimens from the tube-squash test. The hardened cement paste cast in the steel tube and deformed to 50% of its original length is analyzed microscopically to clarify its microstructures. By investigating 50% axially strained cement paste at the microscopic level and comparing it with the mechanical behavior of the concrete filled

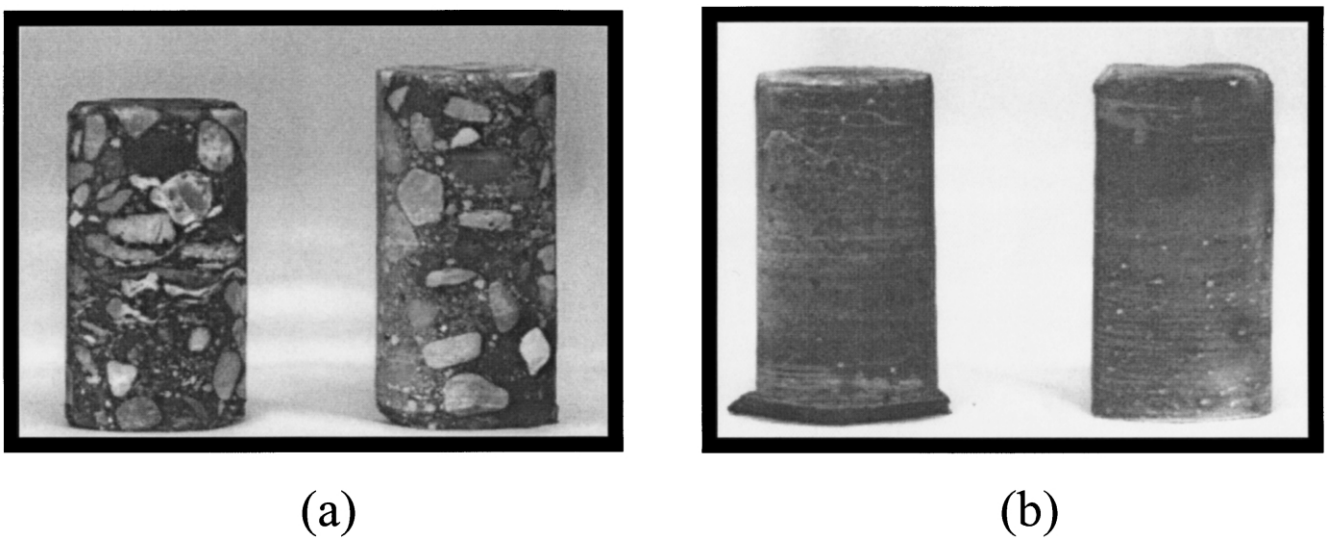

Fig. 5. Cores of deformed and virgin material of (a) HSC and (b) cement paste.

tube specimen, we can relate and separate aggregate and cement matrix contributions to the deformation process and explain the increased ductility of the material.

As explained earlier, the specimens are prepared by slicing cement paste cylinders in the two principal directions of cross-sectional and planar cuts. Since the compression and the deformation of filled tube specimens follow the initial principal axis, the displacement profile can be considered as axis-symmetric.

The focal interest of the research is microscopic analysis of 1-year-old cement paste specimens. Jawed et al. [9] analyzed the hydration of Portland cement by describing C-S-H types in his SEM analysis where he categorized them into four types and described them thus: ''Type I C-S-H is like 'needles radiating from grain', Type II is 'reticulated', Type III is 'indefinite', and Type IV is 'spherical agglomerates'.'' Reinhardt [10] explained the mechanism of hydration of cement focusing on C-S-H production.

For the qualitative analysis, FESEM is performed to compare the morphology of the unstrained (virgin) and strained quasi-brittle concrete materials. Microscopic photos at various magnifications of the concrete materials are taken to observe the constituents (C-S-H hydrate, micropores, microcracks, etc.). It is improper to use FESEM as a quantitative analysis since the results from the analyzed area under the microscope is too small to be representative results of the specimen. However, FESEM visually shows the overall trend of hydrates and microstructures in the specimen. Morphology is really important in this study because the changes in hydrates and microstructures are the important factor in studying the additional ductility in tube-squash test. In the FESEM analysis, various microscopic photos of 3000×, 5000×, 10,000×, 15,000×, and 50,000× magnifications have been taken for cored-out concrete specimen of tube-squash test to clearly observe the hydration products. The 5000× and 10,000× magnification photos are the best resolutions to observe the hydration products. From the 15,000× magnification, the C-S-H hydration products can be clearly observed. Therefore, the photos between 5000× and 10,000× magnification are most suitable to observe several kinds of hydrates in the cement matrix. It is important to note that the ''a tree in a forest'' analogy applies to the analysis since a photo of 15,000× magnification or more can only capture a single kind of hydrates and lose the overall hydration trend of the specimen.

For the quantitative analyses, XRD analysis to compare the relative intensity of $Ca(OH)_2$ among different specimens, DTA/TG to obtain the precise degrees of $Ca(OH)_2$ mass loss, mercury intrusion porosimetry (MIP) to obtain the variation of micropores, and nuclear magnetic resonance spectroscopy (NMR) to extract the very accurate data of Si polymerization degree, are carried out. In tube-squash test, the high compression and large deformation can cause phase changes of hydrates. XRD analyzes the specimen by diffracting X-rays from the surface of crystal where the changes of hydrates can be checked. Also, NMR is used to characterize the extent of hydration and Si polymerization. It is one of the most accurate analyses in qualitative analysis. It is a powerful method for studying the state of Si polymerization, which is closely related to the hydration of specimen. The connectivity of SiO_4 shape obtained from DTA/TG is used to analyze the degree of hydration and Ca/Si ratio. This technique is suitable for an accurate determination of the degree of hydration. In the microlevel analysis in tube-squash test, the degree of hydration is a very important factor due to the way in which the changes contribute to the eventual increase in material ductility. XRD can also analyze the degree of hydration, but it is less accurate than DTA/TG analysis. However, it is useful in analyzing the changing hydration trend during a tube-squash test. NMR also gives the most accurate information of the hydration related to the Si hydrates.

MIP analysis is used to measure the changes in the mesopores, micropores, and microcracks developed in the cement paste specimen. Although MIP analysis cannot effectively measure concrete porosity due to the heterogeneous material characteristic, the results from cement mortar MIP analysis will indirectly provide valuable information in the study. Many changed mesocracks and microcracks during the tube squash test can be observed.

The research procedure for microscopic analysis is as follows.

1. The ''tube-squash'' test and coring is completed 28 days after casting; both virgin and deformed cement paste cores are sliced to produce planar and cross-sectional specimens using a diamond blade saw.
2. Only the midsections are extracted from the previously cut slices of both the planar and cross-sectional specimens. This midsection is where the maximum strain is achieved.
3. The midsections are embedded in epoxy-resin for convenient handling during the grinding and minimum polishing process required for SEM microscopic analysis.
4. A thin layer of Pt–Pd coating is applied to the surface of the specimens.
5. The specimens are stored under vacuum for the best possible observation in FESEM.
6. Microscopic photos are taken of various locations on the specimens using magnifications of 300×, 600×, 5000×, 10,000×, 15,000×, and 50,000×. 300× and 600× magnified photos are taken to observe microcracks and from 5000× magnification, hydrates and micropores are observed.
7. The photos are also taken at various angles with a constant radius from the center of the specimen to show the inherent axis-symmetric geometrical profile.
8. For the 40-day-old planar specimen, the photo-

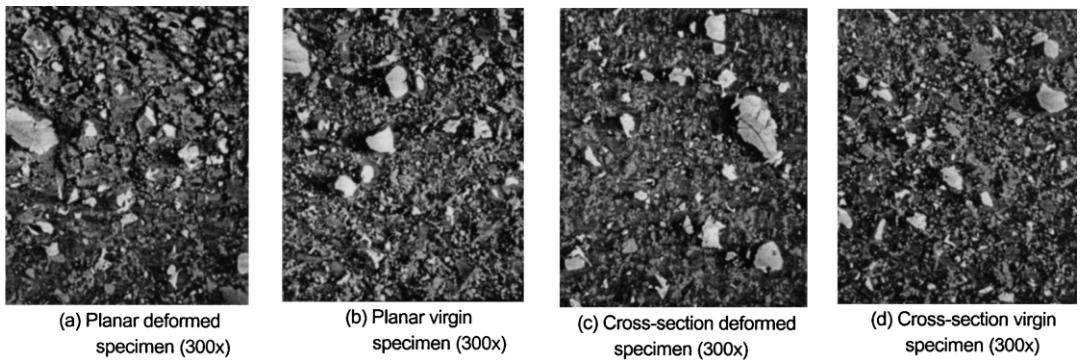

Fig. 6. 40-day-old specimens.

graphed locations are determined by the area where the tensile cracking gradually disappears.

9. EDS analysis is performed of the three-way crack branching area.
10. For the XRD and DTA/TG analyses, the 1-year-old specimens are crushed and ground into very fine powder and are then attached to the receptacle for analysis.

3. Results and discussion

3.1. FESEM analysis

3.1.1. 40-days-old specimen

From the 300× magnification photos of the 40-day-old specimens (Fig. 6), two trends can be observed. The planar photos of virgin and deformed specimens show distinct

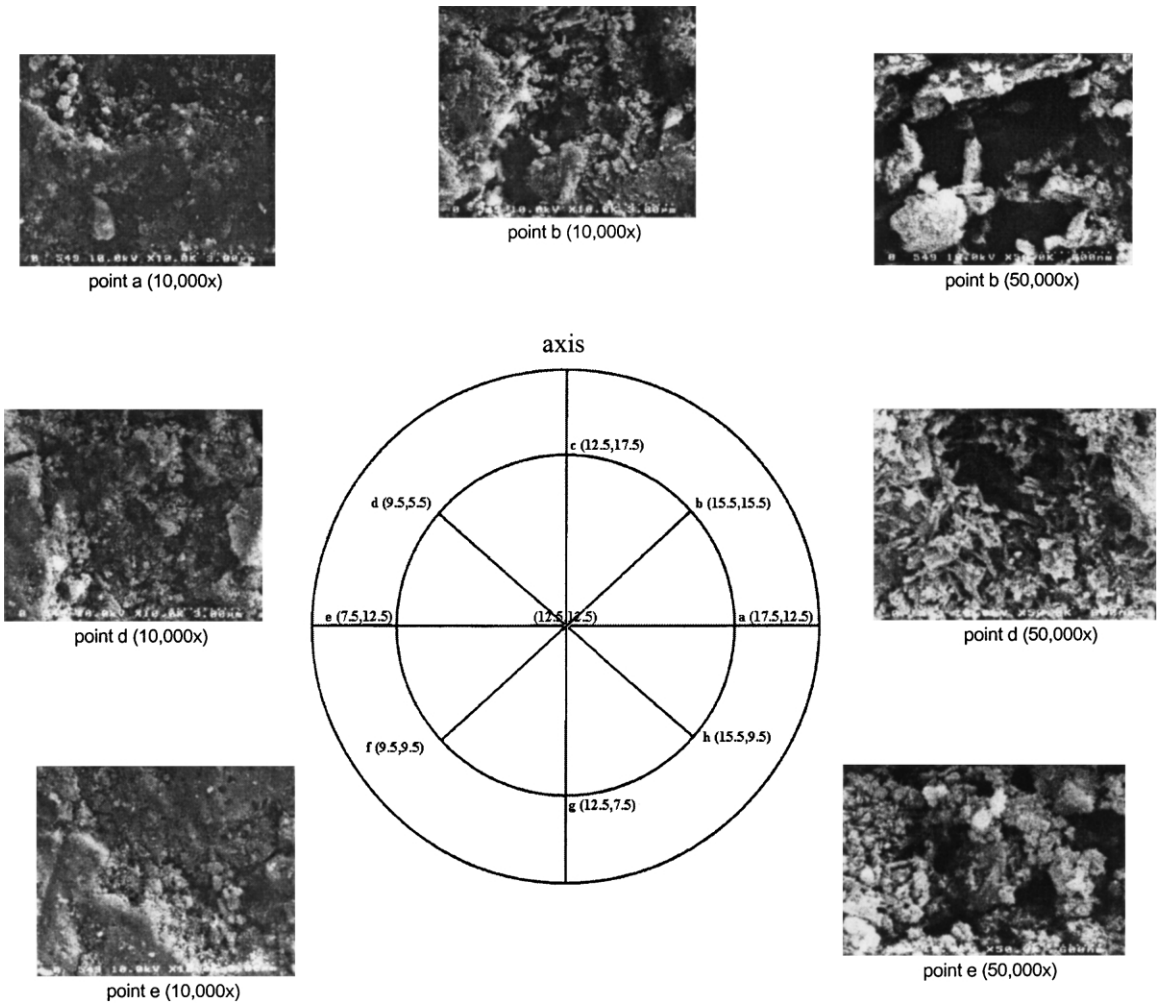

Fig. 7. Planar deformed 1-year-old specimen.

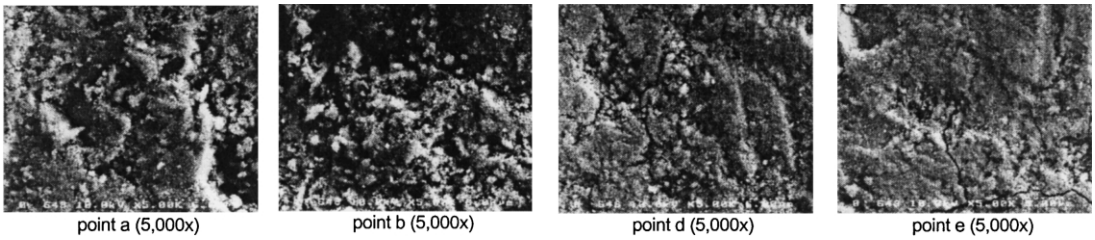

Fig. 8. Cross-section deformed 1-year-old specimen (used same axis as Fig. 7).

differences in their microcrack propagation. Even though microcracks can be detected in the virgin specimen, these cracks are inherent shrinkage cracks rather than tensile strain produced cracks. However, the microcracks observed in the planar deformed specimen are due to large tensile strain in the outer diameter of the midsection, where the microcrack initiates and propagates toward the center of the specimen (Fig. 6(a)). A microscopic photo of the deformed specimen can be divided into three layers. The outermost layer contains several distinct microcracks. As a crack converges toward the center of the specimen, a transition layer emerges where the microcracks gradually disappear. Following the transition layer, the central part of the specimen contains only shrinkage-induced microcracks and tensile cracks do not exist. When photos of the virgin and deformed planar and cross-sectional specimens are com-

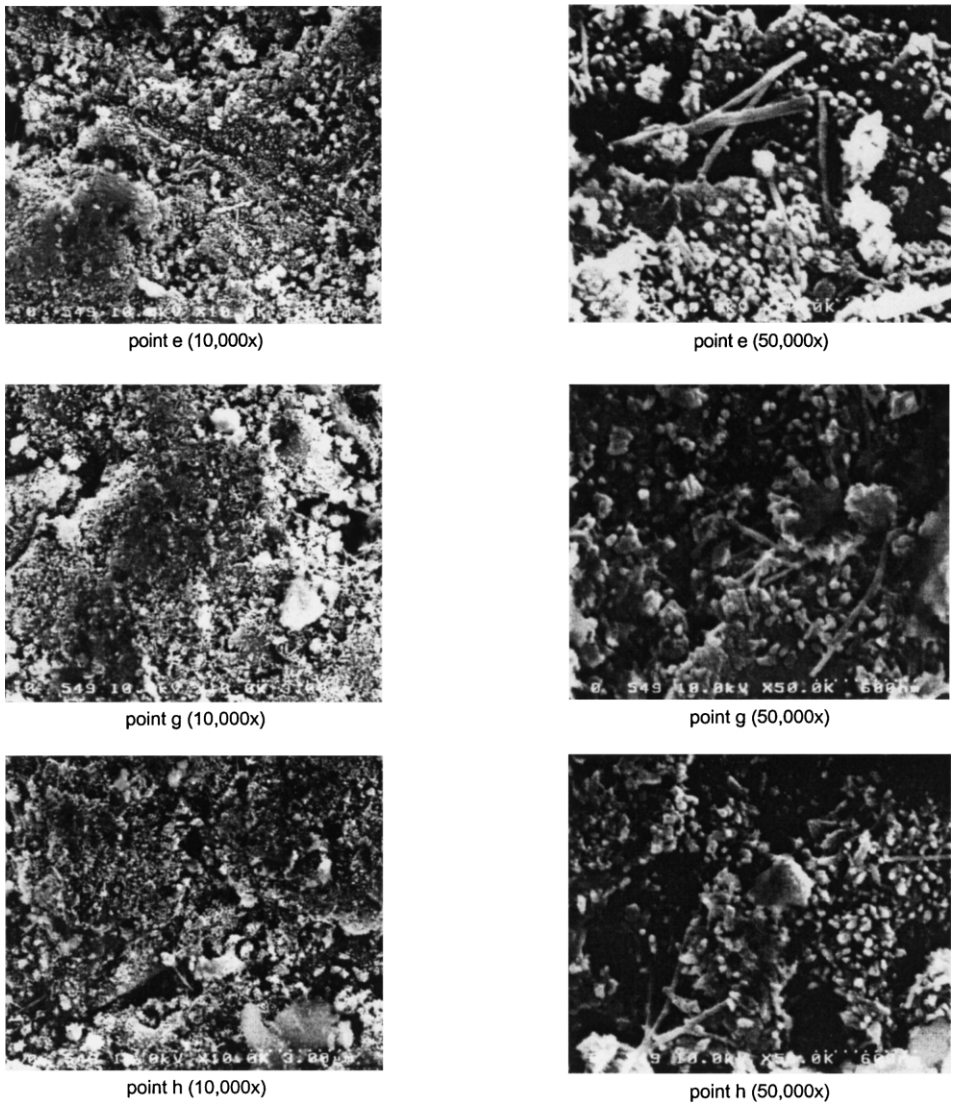

Fig. 9. Planar virgin 1-year-old specimen (used same axis as Fig. 7).

pared, we presume that the rehydration of unhydrated or partially hydrated cement particles has occurred during the 50% axial straining stage. In the virgin specimen photo, light gray dots are scattered throughout the specimen. However, in the deformed specimen, the percentage of light gray dots is smaller and the remaining unhydrated cement particles are converged into larger lumps. In addition, the light gray dots in the transition zone of the planar deformed photograph have a relatively flat shape, differing from the other two zones.

3.1.2. 1-year-old specimen

Photos taken of the 1-year-old specimens with over 5000× magnification are shown in Figs. 7–9. These figures show that the hydration of the 1-year-old specimens is more mature than that of the 40-day-old specimens for both deformed and virgin specimens. There are significant differences between the deformed and virgin specimens in their hydration products (i.e., types and amounts of C-S-H and hydration rate) in both planar and cross-sectional cuts. In the deformed specimen photos (Figs. 10 and 11), we observed a few Type I C-S-H products and the majority were Type III noncrystalline C-S-H. However, in the virgin specimen photos with over 10,000× magnification (Fig. 12), most of the C-S-H products were Type I C-S-H. The planar deformed specimen (Fig. 10) showed an increased amount of Type III C-S-H with a similar "scattered rock formation" appearance. Types I and II C-S-H can also be minutely observed at a few locations. Microcracks and micropores are also observed in the photos. Qualitative observations of the deformed specimens of both planar and cross-sectional cuts show a greater number of micropores than in the virgin specimen. These "rock-shaped" Type III C-S-H products are randomly scattered in the planar deformed specimen (Fig. 7). The figure shows loose microstructures with multiple microcracks and micropores.

Type I C-S-H is observed throughout the planar virgin specimen photo (Fig. 9) with a limited number of Type III. However, the shapes of C-S-H observed in the planar virgin and deformed specimens are noticeably different. The planar virgin specimen has more types of hydration products than does the planar deformed specimen. Similar to the planar deformed specimen (Fig. 7), the planar virgin

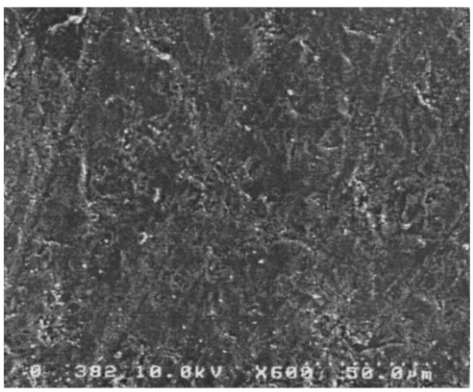

point (6,12) (600x) (planar deformed)

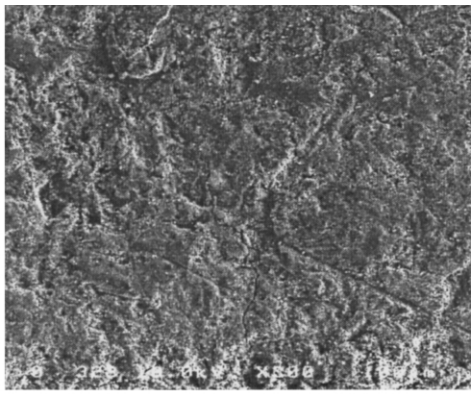

point (0,0) (300x) (planar deformed)

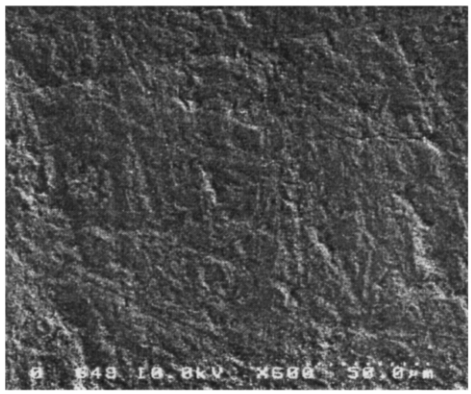

point (7.5,12.5) (600x) (cross-section deformed)

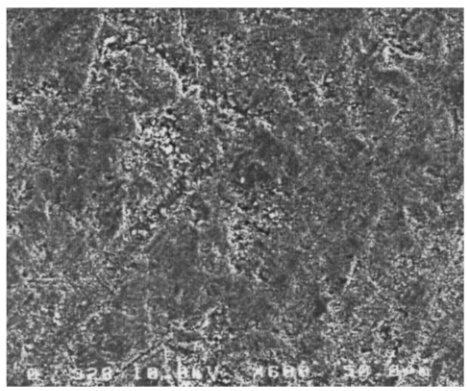

point e (600x) (planar virgin)

Fig. 10. 600× photos of 1-year-old specimen (same axis as Fig. 7).

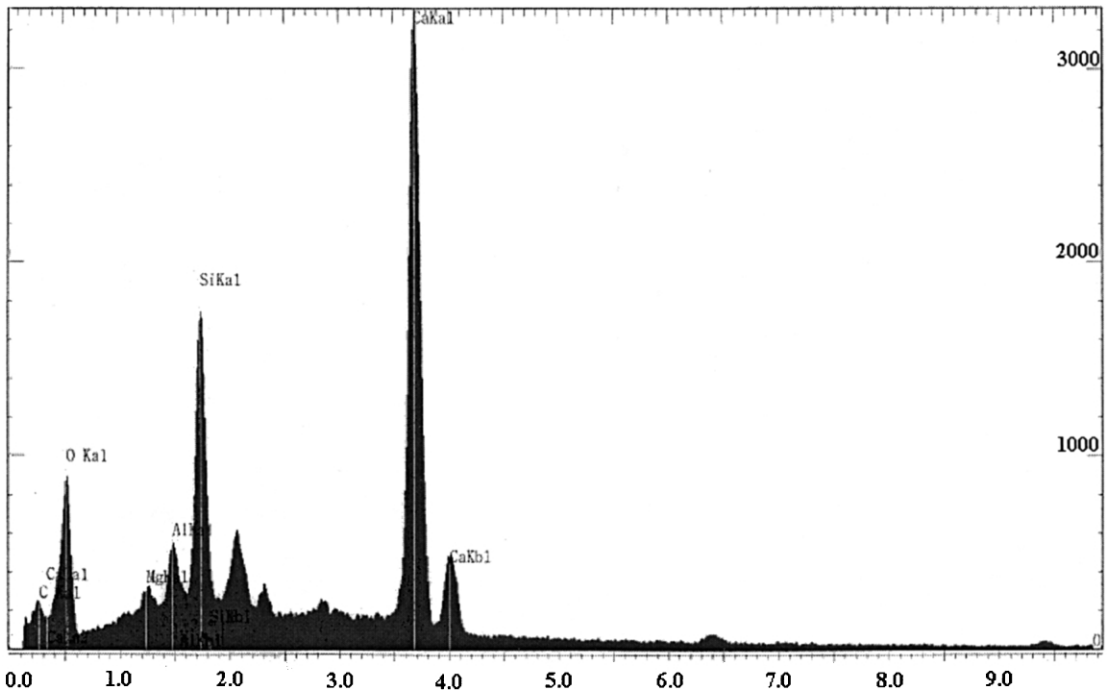

Fig. 11. EDS data.

specimen photo shows an abundant number of microcracks and micropores.

In the cross-sectional deformed specimen (Fig. 8), a similar trend that observed in the planar deformed specimen appears. However, fewer Type III C-S-H are found in the cross-sectional deformed specimen than in the planar one.

Photos taken from 300× and 600× magnifications show several microcracks (Fig. 10). However, these microcracks are not easily located with the naked eye. Unlike the planar deformed 40-day-old specimen, distinct microcracks cannot be found in the outer layer of the planar deformed 1-year-old specimen.

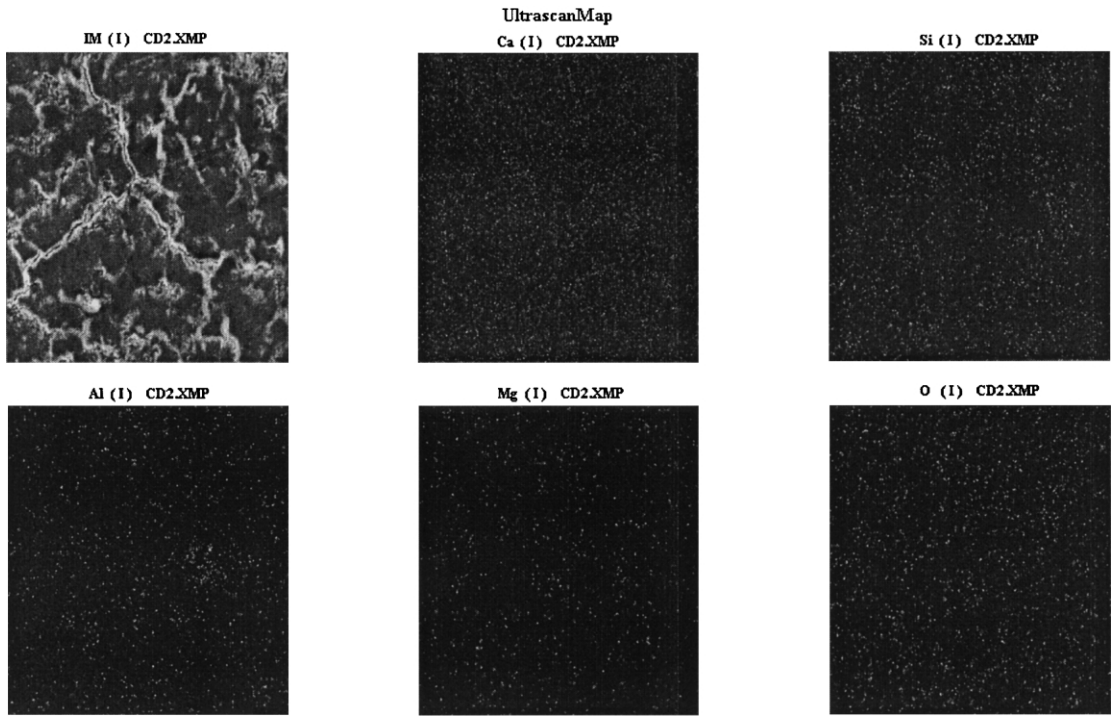

Fig. 12. EDS point mapping.

3.2. EDS analysis

Using the FESEM analysis results, the cracked area of the planar deformed specimen is chosen for EDS analysis (Fig. 11). EDS analysis is normally used to distinguish the different types of hydrates. However, in this research, EDS analysis was performed on the so-called "three-way crack branching" area to check molecular distributions and Ca/Si ratio. As Nemati et al. [11] explained, "three-way crack branching" is one of the well-known crack branching types in brittle materials. From the EDS analysis, the Ca/Si ratio of the deformed 1-year-old specimen ranged between 1.7 and 1.8. This is a similar ratio to that found in normal hardened cement paste. The scattered molecules of Ca and Si are shown in the point-mapping image in Fig. 12, which shows them (the white points are molecules) distributed throughout the captured area. Additionally, the white points found in the Si chart are located in similar positions to the white points found in the Ca chart, although more Ca molecules are found in the chart than Si molecules. If we overlap Si and Al, or Si and Mg charts, fewer white points would overlay each other than in the Ca–Si overlaid chart. The results prove that Al and Mg molecules do not chemically or physically react with Si molecules in cement paste, which is a typical characteristic in cementitious materials.

These results show that the tube-squash test changes the types of hydrates but does not significantly change the molecular distributions. This trend is supported by Fig. 12 where Ca and Si molecules are widely scattered and do not concentrate in one specific area. From these results, we can conclude that the microscopic changes in hardened cement paste applied with finite strain occur at the level of hydrates or microstructure rather than at the molecular level.

3.3. XRD analysis

XRD analysis was performed on the powder made from the cross-sectional and planar 1-year-old deformed and virgin specimens. Fig. 13 shows the different intensities of $Ca(OH)_2$ hydration products in the four specimens taken at angles of 18° and 34°.

The relative intensity of $Ca(OH)_2$ in the cross-sectional virgin specimen powder is higher than that of the cross-sectional deformed virgin specimen powder. The same trend can be observed in a comparison of the planar deformed and virgin specimen powders. This shows that both the amount of hydrate and the degree of hydration of the virgin specimens are different from those of the deformed specimens. The XRD analysis gives an approximate amount of change of the $Ca(OH)_2$ hydrate products. To obtain more accurate information, DTA/TG analysis is performed.

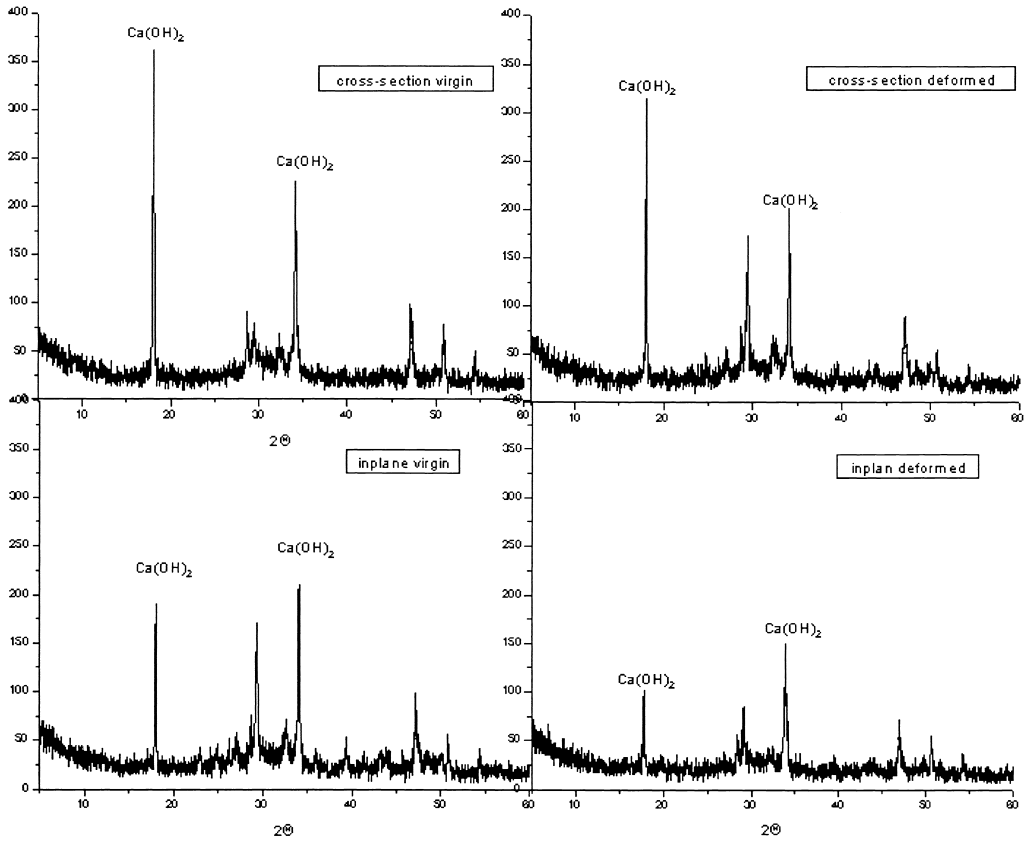

Fig. 13. XRD graph for every type.

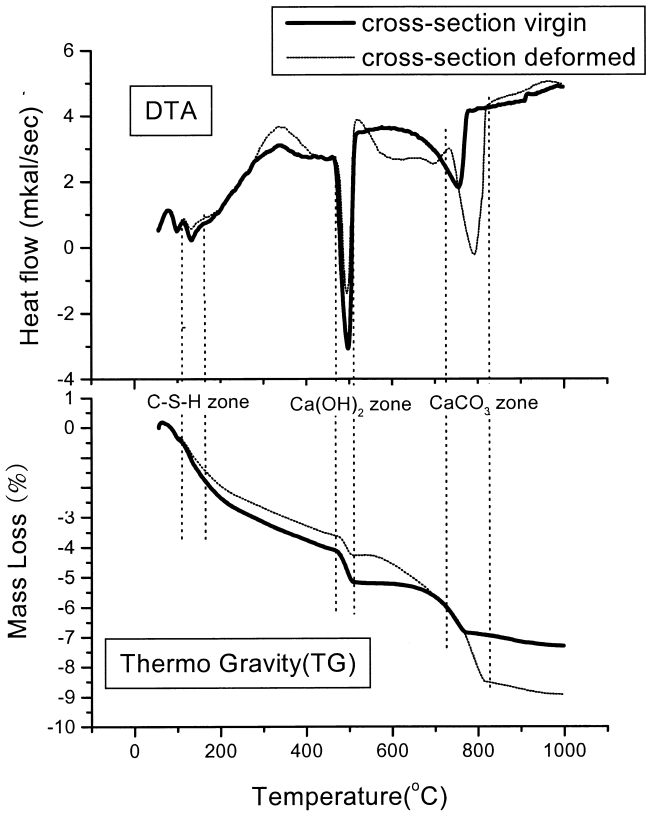

Fig. 14. DTA/TG analysis.

3.4. DTA/TG analysis

DTA/TG analysis was performed on the cross-sectional deformed and virgin cement paste powders from the 1-year-old specimens. As shown in Fig. 14, the degree of hydration of the powder from the virgin specimen is different from that of the deformed specimen powder in the C-S-H and $Ca(OH)_2$ zones. The ratio of mass loss in the $Ca(OH)_2$ zone to total mass loss of the cross-sectional virgin and deformed specimens was 0.166 and 0.083, respectively. The microscopic analysis results clearly show that the degree of hydration of the finitely strained specimen (50% axially strained specimen) changed from the original virgin specimen.

Since the obtained microscopic analysis results are from 1-year-old specimens, it is rather hasty to make a conclusive remark about the relationship between the microscopic structure changes and the tested material property. Therefore, the authors are currently undertaking microscopic analysis of finitely strained 28-day-old specimens. When these results are available, the authors probably can make a conclusive prediction about the relationship.

4. Conclusion

The following conclusions can be drawn from this study.

(1) In the 300× FESEM analysis of the 40-day-old planar deformed specimen, three distinct microstructure layers are observed: (1) an outer layer with the lateral-strain-induced microcracks; (2) a transition layer; (3) and an inner layer with usual shrinkage-induced microcracks. The unhydrated or partially hydrated cement particles are randomly scattered throughout the specimen. In the deformed specimen, the number of observed light gray dots declined and the remaining unhydrated or partially hydrated cement particles converged into larger lumps.

(2) From the FESEM analysis, 5000× magnification photos of the 1-year-old virgin specimen show Types I and III C-S-H. However, photos of the deformed specimen mainly show Type III C-S-H. A greater number of micropores is observed in the deformed specimen than in the virgin specimen. The fact that Type III C-S-H is observed in the 1-year-old deformed specimen proved that many hydrates were crushed during the tube-squash test. The 300× and 600× magnification photos of the 1-year-old specimen showed microcracks that are invisible to the naked eye.

(3) From the EDS analysis, the point-mapping image provided the ratios of Ca and Si and visually showed the locations of various molecules. The results show that the tube-squash test changed the type of hydrates but did not significantly change the molecular distribution. From these results, we can conclude that microscopic changes in a hardened cement paste applied with finite strain occur at the level of hydrates or microstructure rather than at the molecular level.

(4) XRD analysis showed that the amount of hydrate and the degree of hydration in the virgin specimens are higher than those in the deformed specimens. From the DTA/TG analysis, the ratio of mass loss in the $Ca(OH)_2$ zone to total mass loss was 0.166 and 0.083 for the cross-sectional virgin and deformed specimens, respectively. The microscopic analysis results clearly show that the degree of hydration of the finitely strained specimen (50% axially strained specimen) has decreased from the original virgin specimen.

(5) From the microscopic analysis of the finitely strained hardened cement paste, we presume that rehydration of unhydrated or partially hydrated cement particles reoccurred during the 50% axial straining stage. In addition, the distribution of the newly formed and existing hydrates changed. We conclude that the movement and redistribution of the hydrates rather than the actual number of hydrates is the source of increased ductility. However, to propose an exact theory for the behavior of large strained cementitious materials, additional research, including an improved tube squash test, is under way. Results and the proposed theory using the so-called upgraded tube-squash test will be published soon.

Acknowledgments

The support of the Yonsei University for this research is gratefully acknowledged. The financial support to the second author by a fund of National Research Laboratory program of

Year 2000 (2000-N-NL-01-C-162) from Ministry of Science and Technology in Korea is also gratefully appreciated.

References

[1] I.H. Woolson, Some remarkable tests indicating flow of concrete under pressure, Eng. News 54 (18) (1905) 459–460.
[2] G.G. Balmer, Shearing strength of concrete under high triaxial stress computation of Mohr's envelope as curve, Report SP-23, Structural Research Laboratory, Bureau of Reclamation, US. Dept. of the Interior, Denver, CO, 1949.
[3] Z.P. Bazant, Y. Xiang, M.D. Adley, P.C. Prat, S.A. Agers, Microplane model for concrete: Part II. Data delocalization and verification, J. Eng. Mech. Div., Am. Soc. Civ. Eng. 122 (3) (1990) 255–262.
[4] E.G. Burdette, H.K. Hilsdorf, Behavior of laterally reinforced concrete columns, J. Struct. Eng., Am. Soc. Civ. Eng. 97 (2) (1971) 587–602 (Feb.).
[5] R. Park, T. Paulay, Reinforced Concrete Structures, Wiley, New York, 1975.
[6] Z.P. Bazant, F.C. Bishop, T.P. Chang, Confined compression tests of cement paste and concrete up to 3000 ksi, ACI Mater. J. 33 (1986) 553–560 (July–August).
[7] Z.P. Bazant, J.J.H. Kim, M. Brocca, Finite strain tube-squash test of concrete at high pressures and shear angles up to 70 degrees, ACI Mater. J. 96 (1999) 580–592 (September–October).
[8] P.K. Metha, P.J.M. Monteiro, Concrete; Structure, Properties, and Materials, Prentice-Hall, Englewood Cliffs, NJ, 1993.
[9] I. Jawed, J. Skalny, J.F. Young, Hydration of Portland Cement, Structure and Performance of Cements, Applied Science Publishers, London, 1983, pp. 237–317.
[10] H.W. Reinhardt, Relation between the microstructure and structural performance of concrete, in: A. Aguado, R. Gettu, S.P. Shah (Eds.), Concrete Technology: New Trends, Industrial Applications, E&FN Spon, London, 1994, pp. 19–30.
[11] K.M. Nemati, P.J.M. Monteiro, K.L. Scrivener, Analysis of compressive stress-induced cracks in concrete, ACI Mater. J. 95 (1998) 617–630 (September–October).